

# Plasmon-based detection of Uric Acid in aqueous solution using colloidal Ag nanoparticles

Anupam Maity, Sovan Kumar Panda\*

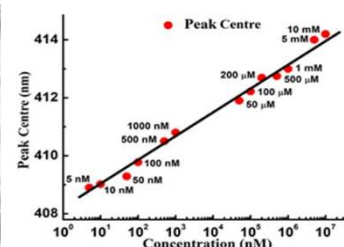
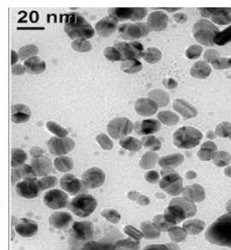
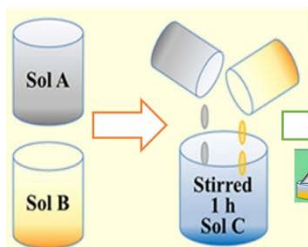
Department of Electronics, Bidhan Chandra College, Rishra, Hooghly, West Bengal, India

Submitted on: 16-Apr-2025, Revised: 22-May-2025, Accepted on: 23-May-2025, Published on: 26-May-2025

Article

## ABSTRACT

Citrate coated stable colloidal silver nanoparticles (Ag NPs) with diameter ranging from 5 to 30 nm were



synthesized by UV-induced citrate reduction of aqueous  $\text{AgNO}_3$  solution. The as-prepared colloid appeared as reddish yellow in colour. The UV-VIS absorption spectrum of the as-prepared colloid exhibited an intense and single plasmonic peak centered at  $\sim 405$  nm implying densely formation of spherical NPs. The colloidal Ag NPs were very stable showing no prominent ageing even after few weeks. The linear red shift of plasmonic peak of Ag NPs was observed in UV-Visible spectroscopy with increase of uric acid concentration in Ag NP-based colloid in the range from 5 nM to 10 mM. This colloidal solution showed excellent sensitivity for uric acid identification and was employed for the quantitative detection of uric acid down to 5 nM limit.

**Keywords:** Colloidal silver nanoparticle, Plasmon-based detection, UV-induced citrate reduction technique, UV-Visible spectroscopy

## INTRODUCTION

Metal nanoparticle-based nanomaterials used as bioanalytical sensor for the qualitative and quantitative detection of biomolecules has attracted attention of scientific communities in recent years.<sup>1-4</sup> Among the metal NPs, noble metal NPs like Ag NPs and Au NPs are promising in term of their properties and performance in the area of biomedical applications. A considerable amount of research has been conducted to synthesize different metallic-nanoparticles.<sup>5-7</sup> but Ag NPs, owing to their excellent chemical reactivity, surface plasmonic resonance (SPR), intense fluorescence properties and antibacterial activities, have been considered as one of the most potential class of materials to be used in pharmaceutical, pathological industries and plasmon based biosensors for the quantitative detection of organic molecules with very high precision.<sup>8-10</sup>

Uric acid is an important organic compound present in human urine and blood. Uric acid serves as immune system stimulant in

human body and it also helps to maintain blood pressure in human body in a salt poor environment. Elevated concentration of uric acid (hyperuricemia) in human body causes formation of sharp crystals in the bone joints and cause gout, a painful form of arthritis. Formation of uric acid crystals in kidneys form kidney stones. Therefore, concentration of uric acid in human body needs to be maintained to stay healthy. The end product of purine metabolic breakdown is uric acid which is very important to maintain its level in human body. Uric acid is also a normal component of human urine and its concentration in blood should be maintained between 2.4-6.0 mg/dL for female and 3.4-7.0 mg/dL for male. Several diseases like leukemia, gout, hyperuricemia, pneumonia, kidney disease, heart disease and diabetes may occur with an increase in concentration of uric acid while its abnormal low concentration may lead to multiple sclerosis.<sup>11-13</sup>

The precise detection of uric acid has been extensively explored by various research groups using diverse nanomaterial-based strategies. Silver nanoparticle-decorated reduced graphene oxide composites have been employed by Kaur *et al.* for this purpose.<sup>9</sup> Another study reports the use of CdTe NPs as fluorescence probes for the quantitative determination of uric acid.<sup>14</sup> A cost-effective, sensitive electrochemical method using a disposable screen-printed carbon electrode modified with graphene nano-sheets and nickel oxide nanoparticles (NiO/GR/SPE) was also developed for the efficient detection of

\*Corresponding Author: Dr. Sovan Panda  
Email: sovan.panda@gmail.com



uric acid.<sup>15</sup> Nanomolar uric acid determination has also been reported by using enlarged gold NPs modified electrode.<sup>16</sup> High-fluorescence sulphur and nitrogen co-doped carbon dots, synthesized via a hydrothermal method, have demonstrated effective uric acid sensing capabilities.<sup>17</sup> Electro-polymerization technique was used to fabricate poly(DPA)SiO<sub>2</sub>@Fe<sub>3</sub>O<sub>4</sub>/CPE which was further applied to estimate uric acid.<sup>18</sup> Additionally, surface-enhanced Raman scattering (SERS) on dried colloidal silver nanoparticle surfaces has been used for the identification of uric acid.<sup>19</sup> Localized surface plasmon resonance (LSPR)-based optical sensors, using radiolytically synthesized silver NPs, were used for estimation of uric acid.<sup>20</sup> A novel optical detection system capable of determination of uric acid in urine sample was described by Azmi *et al.*<sup>21</sup>. Components of human urine like urea, uric acid, creatinine and albumin were investigated using Raman spectroscopy by Premasiri *et al.*<sup>22</sup>

Biosensors based on local surface plasmon resonance technique (LSPR) are simplified and inexpensive alternative over costly and sophisticated detection techniques. The LSPR is based on the oscillation of free electrons present in the conduction band with enhancement of local electromagnetic field. The LSPR phenomenon takes place when the nanoparticle dimension is considerable to the wavelength of the incident electromagnetic wave.<sup>23</sup> At resonance, when the light (either transverse electric or TM) interacts with the metallic nanostructures, a strong plasmonic vibrational peak is observed due to the localization of strong electric field around the metal NP. The resonance condition makes the intensity and wavelength of the localized surface plasmon resonance (LSPR) peak highly sensitive to various factors, including the shape, size, and material of the plasmonic nanostructure, as well as the surrounding medium.

When biomolecules are adsorbed onto the surface of metal nanoparticles (NPs), they alter the local refractive index and dielectric constant at the metal interface. This change leads to a shift in the surface plasmon resonance (SPR) wavelength of the metal. The magnitude of this wavelength shift is quantitative and directly correlates with the amount of bound biomolecules.

With the advancement of science and technology and the increasing demand of cost-effective material in market for the fabrication of biosensors is of immense importance now a days. The drawback of complex labeling protocol, complex instrumentation, expensive procedure requiring considerable amount of sample volumes that can be overcome with LSPR based sensor. It offers the advantage of easy multiplexing with high output sensing even up-to zeptomole range.<sup>24</sup> However, demand of a simple, cost effective and fast detection of organic molecules with excellent sensitivity is always there in the pathological laboratories, forensic science and food industries to determine the trace amount of impurities at low cost. UV-VIS spectroscopy can be used in this regard where absorption spectrum of plasmonic NPs like Ag or Au is studied and quantitative detection of organic molecules can be performed by studying the absorption spectrum of the NPs in the presence of bio-molecules. Qualitative or quantitative detection of organic molecules can be achieved through their interaction with nanoparticles (NPs). Upon interaction with the sensing

biomolecules, NPs may form aggregates of varying sizes, leading to multi-dimensional dispersion. This often results in a broadening of the LSPR band and/or a red shift in its peak position and sometimes visible colour change in the solution. In other cases, the optical response may differ, with the LSPR band shifting toward shorter wavelengths (blue shift) and, in some instances, a reduction in band intensity. Thus, from the broadening/shifting of peak centre/variation of intensity of main plasmonic peak/colour change of the colloid, quantitative detection is carried out.

There have been several techniques like electrochemical deposition, chemical reduction method, physical vapor deposition etc. reported in the literature for the synthesis of Ag NPs.<sup>25–28</sup> The chemical reduction method has been widely studied due to its advantages, including the ability to produce colloidal nanoparticles (NPs) with minimal aggregation and its suitability for low-cost, large-scale production. This technique typically involves the reduction of metal salts, such as silver nitrate (AgNO<sub>3</sub>), using appropriate reducing agents<sup>29</sup> Among a number of wet chemical reduction techniques by which colloidal Ag NPs can be prepared, citrate reduction technique is an important one since in this process citrate ions not only reduces the metal salt to produce Ag NPs but also acts as capping layer and prevent the NPs from aggregation. The synthesis protocol of producing colloidal Ag NPs with UV-induced citrate reduction technique provides the advantage with room temperature synthesis of Ag NPs by reducing aqueous AgNO<sub>3</sub> using sodium citrate (C<sub>6</sub>H<sub>5</sub>Na<sub>3</sub>O<sub>7</sub>) where Ag<sup>+</sup> is reduced to Ag<sup>0</sup> and the citrate acts as a stabilizer by coating the NPs by (citrate)<sup>-</sup> ions

In this paper, we report the facile, one step and environment friendly synthesis of UV-induced citrate reduction technique to produce colloidal Ag NPs at room temperature for the detection of uric acid by studying the plasmonic absorption of colloidal Ag NPs using UV-VIS spectroscopy.

## EXPERIMENTAL DETAILS

### Synthesis

For the synthesis of Ag NPs, 99.99% pure silver nitrate (AgNO<sub>3</sub>) was dissolved in deionized water and stirred at 360 rpm for 15 min at room temperature to prepare 0.5 mM (mili mole) aqueous AgNO<sub>3</sub> solution (Solution A). Another solution was prepared by dissolving tri-sodium citrate (C<sub>6</sub>H<sub>5</sub>Na<sub>3</sub>O<sub>7</sub>) in deionized water and stirred properly to get 0.5 wt% aqueous sodium citrate solution (Solution B). Then, 60 ml of solution A was mixed with 0.6 ml of Solution B and stirred for 1 hour at room temperature (Solution C). The homogeneous mixture (Solution C) was then poured on a glass petri dish with open lid and exposed for 2 hour and 30 minutes under UV light comprising of wavelength ~ 360 nm and power ~ 8 mW. The schematic representation of synthesis mechanism is depicted in Figure 1. The formation of Ag NPs was confirmed by a transformation of colorless solution to reddish yellow colored colloid. The colloid was then stored at 293 K for few weeks to perform ageing measurements.

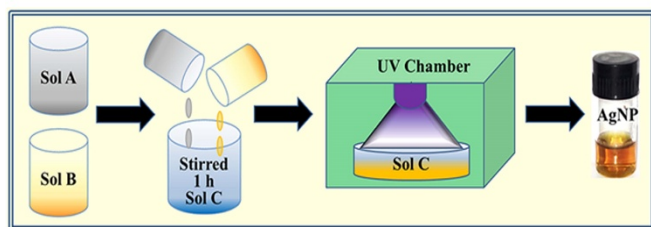


**Figure 1:** Schematic representation of synthesis mechanism of colloidal Ag NPs by UV-induced citrate reduction technique.

### Characterizations

As prepared colloid and the colloid preserved for 50 days were characterized by using UV-VIS spectro-photometer (Agilent Technologies Cary 60 UV-VIS, Spectral resolution  $\sim 0.1$  nm) in the 200-800 nm range. Particle size distribution and micro-structural study of the NPs were carried out by using JEM 2010 transmission electron microscope (TEM) operated at 200 kV. For TEM characterization, sample was prepared by placing two drop of Ag colloid on the carbon coated holey Copper grid and drying it normally in air. Dynamic light scattering (DLS) (SZ-100, Horiba Scientific – Japan) was used to further confirm the particle size distribution of the as-synthesized Ag NPs.

### Uric acid detection method

Desired concentrations of aqueous uric acid solutions (5 nM to 10 nM) were prepared and mixed with as-prepared Ag NPs colloid at 1:9 (v/v) ratios. UV-VIS absorption study of this solution (uric acid and Ag NPs) was then performed with wavelength ranging from 200 to 800 nm.

## RESULTS AND DISCUSSION

Figures 2 (a, b and c) show the optical images of as-prepared colloid obtained from UV-induced citrate reduction technique and preserved colloid after 25 and 50 days, respectively. The deep reddish yellow colour of Figure 2 (a) stipulates dense formation of spherical silver NPs in the colloid.<sup>29,30</sup> However, the reddish yellow colour did not change significantly with time as shown in Figures 2 (b) & (c) even after 25 and 50 days, respectively, indicating that the NPs are very stable and don't agglomerate to form larger particles or degrade over the passage of time when kept at 293 K.

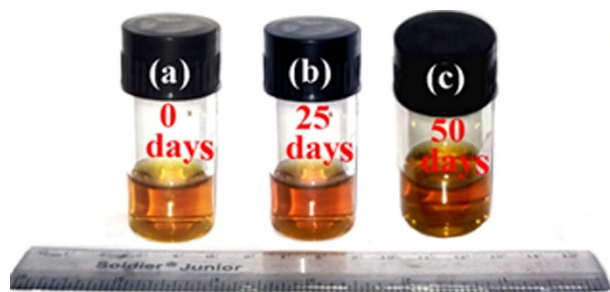


**Figure 2:** Optical image of (a) As prepared colloid (b) Colloid after 25 days, (c) Colloid after 50 days.

In order to confirm the formation of Ag NPs, UV-VIS absorption study was further demonstrated which is shown in Figure 3. The UV-VIS spectrum illustrates the presence of an

intense and single absorption peak centered at  $\sim 405$  nm. The absorption peak is due to the dipole resonance being created by the collective oscillations of the conduction electrons of NPs in phase with the frequency of the incident light. It is well-known that the peak position of UV spectra is linked with the size of the NPs present.<sup>31</sup> For small spherical NPs, the charges are displaced homogeneously which results one proper resonance.<sup>32</sup> The presence of single intense plasmonic absorption peak at  $\sim 405$  nm in the spectrum, known as the characteristic plasmon peak of Ag NPs, designate the formation of dense and fine-spherical NPs.<sup>33,34</sup> NPs with lower symmetry have nonuniform electron distribution and may results quadrupole plasmonic vibration showing complex features and illustrate multiple absorption whereas the size of the nanoparticles determine the position of the absorption peak.<sup>35,36</sup> However, single absorption peak rules out the formation of low symmetry features in the colloid.

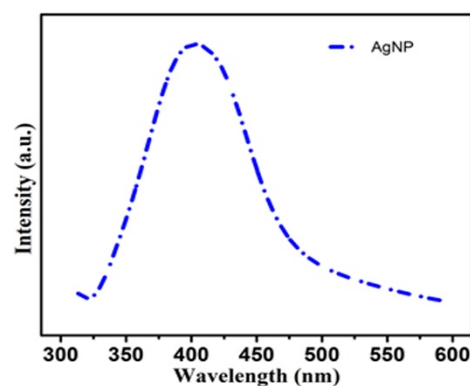


**Figure 3:** UV-VIS absorption spectrum of as-prepared colloidal Ag NPs

The ageing study of the Ag NPs is shown in Figure 4. UV-VIS absorption study doesn't show significant shifting of absorption peak centre and no change in the shape of the plasmonic absorption peak even after 50 days indicating stability of the NPs and stipulating that the NPs were not agglomerated to form larger particles. The intensity of the absorption peak didn't change over the investigated time span commanding that the NP number density remained unaltered over the period which is also in agreement with the optical photograph of Figure 2 (a-c).

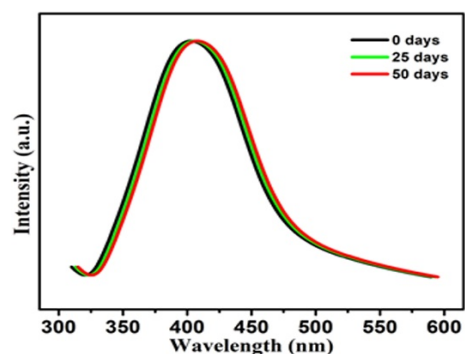


**Figure 4:** Ageing study of freshly prepared colloid, the colloid after 25 days and the colloid after 50 days.

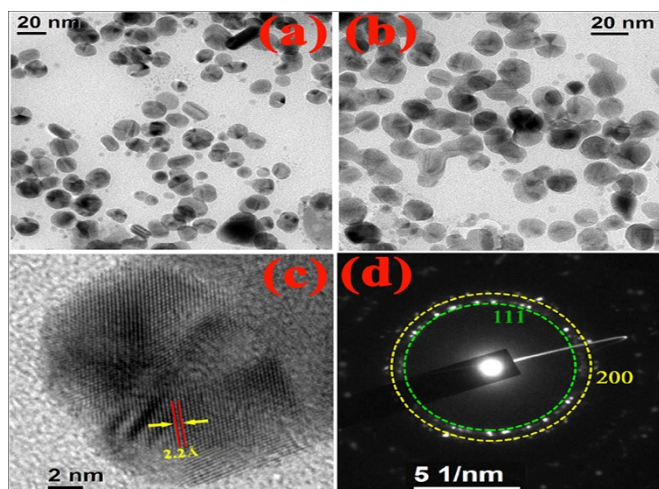
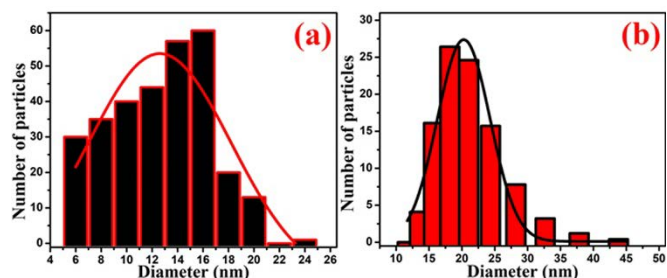


**Figure 5:** (a) & (b) Bright field TEM image of Ag NPs with different magnifications. (c) HRTEM image of a single NP showing the lattice fringe (d) SAED pattern from the NPs.

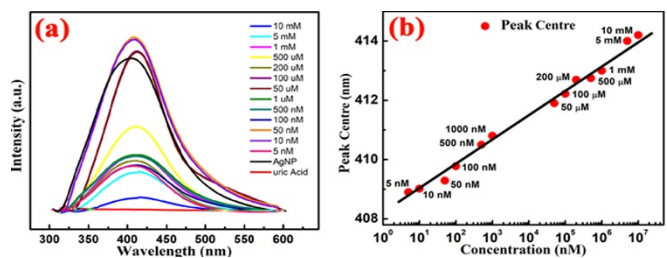
Figures 5 (a & b) show the bright field transmission electron micrographs (HRTEM) of the as-prepared Ag NPs which clearly illustrate the formation of spherical NPs having diameter within the range of 5 to 30 nm. Few elongated NPs were also noticed in the micrograph which may have formed due to aggregation of spherical particles during sample preparations for TEM study. TEM study further confirms the argument of UV-VIS study on the shape and size of the NPs. Figures 5 (c & d) show the HRTEM lattice image and SAED pattern obtained from the Ag NPs. The lattice planes were identified from HRTEM image by measuring the d-spacing values of  $\sim 2.2\text{\AA}$  which is corresponding to cubic Ag (111) planes. The SAED pattern was also indexed with respect to the JCPDS Card No. 04-0783, confirming the presence of single crystalline (cubic) Ag NPs. However, the ring pattern may have appeared due to the presence of a number of NPs within the beam diameter of TEM system. The particle size distribution was obtained from TEM image of Figure 5 (a) by using ImageJ 1.37v and is shown in Figure 6 (a). From the particle distribution pattern, the mean diameter of the NPs was obtained using Gaussian distribution function and the central distribution was found to be  $\sim 13$  nm. Real time particle size distribution of the NPs inside the colloid was further determined by DLS study which is depicted in Figure 6 (b). DLS study further reveals that the NPs have narrow size distribution with the mean particle diameter  $\sim 20$  nm which is in close agreement to the mean diameter obtained from TEM image.

Figure 7 (a) demonstrates the UV-VIS absorption spectra of colloidal Ag NPs in the presence of aqueous uric acid solution with concentrations ranging from 5 nM to 10 mM. It is observed that with increasing concentrations of uric acid, center of plasmonic absorption band shifted towards longer wavelength (red shift) with a significant reduction of peak intensity. Red shift of plasmonic band may be ascribed to the partial oxidation of Ag NPs.<sup>37-40</sup> or it might be a result of small aggregation of these NPs formed due to the rupture of the citrate shell stabilizing the NPs in presence of uric acid.<sup>41</sup> However, in this study, it is

thought that uric acid being a nitrogen containing compound, when mixed with citrate capped Ag NPs, nitrogen components are adsorbed on the surface of Ag NPs, partially breaking the citrate capping.



**Figure 6:** (a) Particle size distribution pattern obtained from TEM images of Figure 5 (a), Solid line curve represents the Gaussian fit. (b) DLS study of as-prepared colloidal Ag NPs, solid line curve represents the Gaussian fit.



**Figure 7:** (a) Absorption spectra of the colloidal Ag NPs in the presence of uric acid with concentrations ranging from 5 nM to 10 mM. (b) Plot of absorption peak centers with the increase of concentration of uric acid.

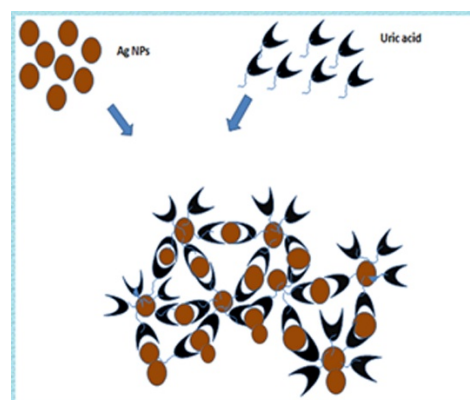


**Figure 8:** Proposed cluster formation mechanism of Ag NPs in the presence of uric acid.

As a result, uncoated or partially coated NPs into the colloid coalesce to form larger NP/cluster by Ostwald ripening mechanism which in turn shifts the plasmonic absorption peak towards the longer wavelength region causing a red shift of the plasmonic absorption peak center.<sup>42</sup> The possible cluster formation mechanism of Ag NPs in presence of uric acid is shown in Figure 8. A linear variation of the peak center with increasing concentration of uric acid from 5 nM to 10 mM was observed. With increase of uric acid concentration, cluster density increases and hence the linear shift of absorption band

was observed. However, the prepared colloidal Ag NPs are capable of sensing uric acid over a wide range of concentration and minimum concentration was measured in this method was ~ 5 nM which is quite impressive. The study was reproducible with the variation within the tolerance limit.

## CONCLUSIONS

Colloidal silver nanoparticles with diameter ranging from 5 to 30 nm were synthesized successfully by UV-induced citrate reduction technique. The yellow-colored colloid constituted of dense, spherical, single crystalline Ag NPs only. The as prepared NPs showed excellent stability due to citrate capping even after 50 days. As-prepared colloidal Ag NPs are capable of detecting uric acid over a wide range of 5 nM to 10 mM. The colloidal Ag-NP-based detecting system shows excellent sensitivity down to ~ 5 nM limit. The facile synthesis procedure of Ag NPs at room temperature for the quantitative detection of uric acid by plasmon-based technique in the nanomolar to milimolar range.

## ACKNOWLEDGMENTS

The authors sincerely acknowledge the financial support of DST-INSPIRE Faculty Project (IFA 12-ENG-17, 2012), New Delhi and ANRF, DST (TAR/2023/000031), Govt. of India, for this work.

## CONFLICT OF INTEREST STATEMENT

The corresponding author, on behalf of all authors, declare that there is no conflict of interest.

## REFERENCES AND NOTES

- S. Schultz, D.R. Smith, J.J. Mock, D.A. Schultz. Single-target molecule detection with nonbleaching multicolor optical immunolabels. *Proc. Natl. Acad. Sci. U. S. A.* **2000**, 97 (3), 996–1001.
- T.A. Taton, C.A. Mirkin, R.L. Letsinger. Scanometric DNA array detection with nanoparticle probes. *Science* (80-. ). **2000**, 289 (5485), 1757–1760.
- J. Yguerabide, E.E. Yguerabide. Light-scattering submicroscopic particles as highly fluorescent analogs and their use as tracer labels in clinical and biological applications II. Experimental characterization. *Anal. Biochem.* **1998**, 262 (2), 157–176.
- G. V. Ramesh, S. Porel, T.P. Radhakrishnan. Polymer thin films embedded with in situ grown metal nanoparticles. *Chem. Soc. Rev.* **2009**, 38 (9), 2646–2656.
- G.L. Hornyak, C.J. Patrissi, C.R. Martin. Fabrication, characterization, and optical properties of gold nanoparticle/porous alumina composites: The nonscattering Maxwell-Garnett limit. *J. Phys. Chem. B* **1997**, 101 (9), 1548–1555.
- J. Singh, T. Dutta, K.H. Kim, et al. “Green” synthesis of metals and their oxide nanoparticles: Applications for environmental remediation. *J. Nanobiotechnology* **2018**, 16 (1), 84.
- B. Wang, S. Li, J. Liu, M. Yu. Preparation of nickel nanoparticle/graphene composites for non-enzymatic electrochemical glucose biosensor applications. *Mater. Res. Bull.* **2014**, 49 (1), 521–524.
- A. Maity, S.K. Panda. Colloidal silver nanoparticles prepared by UV-light induced citrate reduction technique for the quantitative detection of uric acid. *AIP Conf. Proc.* **2018**, 1942, 050057.
- B. Kaur, T. Pandiyan, B. Satpati, R. Srivastava. Simultaneous and sensitive determination of ascorbic acid, dopamine, uric acid, and tryptophan with silver nanoparticles-decorated reduced graphene oxide modified electrode. *Colloids Surfaces B Biointerfaces* **2013**, 111, 97–106.
- S. Meenakshi, S. Devi, K. Pandian, R. Devendiran, M. Selvaraj. Sunlight assisted synthesis of silver nanoparticles in zeolite matrix and study of its application on electrochemical detection of dopamine and uric acid in urine samples. *Mater. Sci. Eng. C* **2016**, 69, 85–94.
- E. Miller, J. Kędziora. Effect of whole body cryotherapy on uric acid concentration in plasma of multiple sclerosis patients. *Int. Rev. Allergol. Clin. Immunol.* **2011**, 17 (1–2), 20–23.
- A. Dang, Y. Zhang, G. Liu, et al. Effects of losartan and irbesartan on serum uric acid in hypertensive patients with hyperuricaemia in Chinese population. *J. Hum. Hypertens.* **2006**, 20 (1), 45–50.
- R. Mohandas, R.J. Johnson. Uric acid levels increase risk for new-onset kidney disease. *J. Am. Soc. Nephrol.* **2008**, 19 (12), 2251–2253.
- D. Jin, M.H. Seo, B.T. Huy, et al. Quantitative determination of uric acid using CdTe nanoparticles as fluorescence probes. *Biosens. Bioelectron.* **2016**, 77, 359–365.
- S. Jahani, H. Beitollahi. Selective Detection of Dopamine in the Presence of Uric Acid Using NiO Nanoparticles Decorated on Graphene Nanosheets Modified Screen-printed Electrodes. *Electroanalysis* **2016**, 28 (9), 2022–2028.
- P. Kannan, S.A. John. Determination of nanomolar uric and ascorbic acids using enlarged gold nanoparticles modified electrode. *Anal. Biochem.* **2009**, 386 (1), 65–72.
- H. Wang, Q. Lu, Y. Hou, Y. Liu, Y. Zhang. High fluorescence S, N co-doped carbon dots as an ultra-sensitive fluorescent probe for the determination of uric acid. *Talanta* **2016**, 155, 62–69.
- Y. Veera Manohara Reddy, B. Sravani, S. Agarwal, V.K. Gupta, G. Madhavi. Electrochemical sensor for detection of uric acid in the presence of ascorbic acid and dopamine using the poly(DPA)/SiO<sub>2</sub>@Fe<sub>3</sub>O<sub>4</sub> modified carbon paste electrode. *J. Electroanal. Chem.* **2018**, 820, 168–175.
- M. Pucetaite, M. Velicka, J. Pilipavicius, et al. Uric acid detection by means of SERS spectroscopy on dried Ag colloidal drops. *J. Raman Spectrosc.* **2016**, 47 (6), 681–686.
- N. Misra, V. Kumar, L. Borde, L. Varshney. Localized surface plasmon resonance-optical sensors based on radiolytically synthesized silver nanoparticles for estimation of uric acid. *Sensors Actuators, B Chem.* **2013**, 178, 371–378.
- N.E. Azmi, N.I. Ramli, J. Abdullah, et al. A simple and sensitive fluorescence based biosensor for the determination of uric acid using H<sub>2</sub>O<sub>2</sub>-sensitive quantum dots/dual enzymes. *Biosens. Bioelectron.* **2015**, 67, 129–133.
- P.W.A. Willems, W. Peter Vandertop, R.M. Verdaasdonk, C.F.P. Van Swol, G.H. Jansen. Urine analysis by laser Raman spectroscopy. *Lasers Surg. Med.* **2001**, 28 (4), 330–334.
- R.A. Alvarez-Puebla. Surface Enhanced Raman Spectroscopy (SERS); Wiley-VCH Verlag GmbH & Co. KGaA, Weinheim, Germany, **2023**.
- A.D. McFarland, R.P. Van Duyne. Single silver nanoparticles as real-time optical sensors with zeptomole sensitivity. *Nano Lett.* **2003**, 3 (8), 1057–1062.
- Z.S. Pillai, P. V. Kamat. What factors control the size and shape of silver nanoparticles in the citrate ion reduction method? *J. Phys. Chem. B* **2004**, 108 (3), 945–951.
- S.D. Solomon, M. Bahadory, A. V. Jeyarajasingam, et al. Synthesis and study of silver nanoparticles. *J. Chem. Educ.* **2007**, 84 (2), 322–325.
- F. Giorgis, E. Descrovi, A. Chiodoni, et al. Porous silicon as efficient surface enhanced Raman scattering (SERS) substrate. *Appl. Surf. Sci.* **2008**, 254 (22), 7494–7497.
- M. Raffi, F. Hussain, T.M. Bhatti, et al. Antibacterial characterization of silver nanoparticles against E.coli ATCC-15224. *J. Mater. Sci. Technol.* **2008**, 24 (2), 192–196.
- S.K. Panda, S. Sen, S. Roy, A. Moyez. Synthesis of Colloidal Silver Nanoparticles by Reducing Aqueous AgNO<sub>3</sub> Using Green Reducing Agents. *Mater. Today Proc.* **2018**, 5 (3), 10054–10061.
- B.J. Wiley, S.H. Im, Z.Y. Li, et al. Maneuvering the surface plasmon resonance of silver nanostructures through shape-controlled synthesis. *J. Phys. Chem. B* **2006**, 110 (32), 15666–15675.

31. S.K. Panda, S. Chakraborti, R.N. Basu. Size and shape dependences of the colloidal silver nanoparticles on the light sources in photo-mediated citrate reduction technique. *Bull. Mater. Sci.* **2018**, 41 (4), 90–.
32. C. Noguez. Surface plasmons on metal nanoparticles: The influence of shape and physical environment. *J. Phys. Chem. C* **2007**, 111 (10), 3606–3619.
33. K.C. Song, S.M. Lee, T.S. Park, B.S. Lee. Preparation of colloidal silver nanoparticles by chemical reduction method. *Korean J. Chem. Eng.* **2009**, 26 (1), 153–155.
34. A.L. González, C. Noguez, J. Beránek, A.S. Barnard. Size, shape, stability, and color of plasmonic silver nanoparticles. *J. Phys. Chem. C* **2014**, 118 (17), 9128–9136.
35. I.O. Sosa, C. Noguez, R.G. Barrera. Optical properties of metal nanoparticles with arbitrary shapes. *J. Phys. Chem. B* **2003**, 107 (26), 6269–6275.
36. A. Rai, A. Singh, A. Ahmad, M. Sastry. Role of halide ions and temperature on the morphology of biologically synthesized gold nanotriangles. *Langmuir* **2006**, 22 (2), 736–741.
37. A. Henglein. Colloidal Silver Nanoparticles: Photochemical Preparation and Interaction with O<sub>2</sub>, CCl<sub>4</sub>, and Some Metal Ions. *Chem. Mater.* **1998**, 10 (1), 444–450.
38. A. Henglein. Physicochemical properties of small metal particles in solution: “Microelectrode” reactions, chemisorption, composite metal particles, and the atom-to-metal transition. *J. Phys. Chem.* **1993**, 97 (21), 5457–5471.
39. X. Li, J.J. Lenhart, H.W. Walker. Dissolution-accompanied aggregation kinetics of silver nanoparticles. *Langmuir* **2010**, 26 (22), 16690–16698.
40. C.N. Lok, C.M. Ho, R. Chen, et al. Silver nanoparticles: Partial oxidation and antibacterial activities. *J. Biol. Inorg. Chem.* **2007**, 12 (4), 527–534.
41. P. Vasileva, B. Donkova, I. Karadjova, C. Dushkin. Synthesis of starch-stabilized silver nanoparticles and their application as a surface plasmon resonance-based sensor of hydrogen peroxide. *Colloids Surfaces A Physicochem. Eng. Asp.* **2011**, 382 (1–3), 203–210.
42. Z.X. Wang, S.N. Ding. A simple colorimetric detection of silver ion based on uric acid for plasmonic silver nanoparticle. *Environ. Energy Appl. Technol. - Proc. 2014 3rd Int. Conf. Front. Energy Environ. Eng. ICFEET 2014* **2015**, 123–127.